Kink walls and critical behavior of magnetization near the lock-in transition in layered superconductors

A. E. Koshelev*
Kamerlingh Onnes Laboratory, Leiden University, P.O. Box 9506, 2300 RA Leiden, The Netherlands
(Received 9 November 1992; revised manuscript received 22 January 1993)

We consider the behavior of a layered superconductor in a magnetic field applied at very small angles with respect to the layers. The penetration of the field component perpendicular to the layers occurs as a result of the phase transition (lock-in transition). The boundary of the locked phase is calculated exactly. We argue that the penetration of the transversal field occurs by the formation of separated kink walls. The structure of field in the wall and the behavior of magnetization depend essentially upon the value of the field along layers B_x. At small B_x a kink wall is composed of separated magnetic flux tubes. Each tube contains flux that depends upon B_x and smaller than a flux quantum. At large B_x these tubes overlap and form a magnetic flux wall. The behavior of the magnetization near the transition is studied in detail. At large separations between kink walls they interact exponentially and their concentration sharply increases in the narrow region above the lock-in field. This leads to the appearance of a tiny peak in the field dependence of the magnetization, which can be used to indicate the lock-in transition.

I. INTRODUCTION

The discovery of high-T_c superconductors triggered new development in the phenomenological theory of layered superconductors. It is well established at present that high-T_c superconductors can be described phenomenologically as a stack of two-dimensional (2D) superconducting layers weakly coupled by Josephson interactions. Each superconducting layer consists of one or several CuO_2 planes. The strength of the Josephson coupling varies in wide limits depending upon the compound.

Layered superconductors have a very peculiar behavior in a magnetic field applied almost parallel to the layers (the geometry is shown in Fig. 1). The expected behavior in an ideal superconductor (i.e., without pinning centers) at low temperatures can be described as follows. When the magnetic field is applied exactly parallel to the layers the stretched triangular lattice of the Josephson vortices appears. At small tilting angles of the external field with respect to the *ab* plane the vortex lattice remains oriented along the layers and the *z* component of the external field, $H_z^{\rm ext}$, is completely screened ("locked-vortex-lattice" phase). The penetration of $H_z^{\rm ext}$ occurs as a result of the phase transition when the *z* component of the internal field H_z exceeds the critical value $H_{\rm lock\ in}$ ("lock-in" transition). The penetration of field occurs through the formation of kinks in the vortex lattice (the kink is a point defect that separates two pieces of a Josephson vortex shifted at a distance of one interlayer separation in the *z* direction). The *z* component of the field starts to penetrate when the gain in energy due to the penetration of the field exceeds the loss in energy due to the formation of kinks.

This physical picture was proposed by Feinberg and Villard.[1] The model used in these papers gives a correct qualitative picture but it is too rude to provide a quantitative description of the transition. The reason is that the authors neglected nonlocality in the tilt stiffness of the lattice and took into account the layered structure by introducing phenomenologically the cosine periodic potential. A more quantitative approach was elaborated in the later papers,[2-5] where the energy of the kinked lattice and the field dependence of the magnetization were estimated using the 3D anisotropic London model[2,3] and the Lawrence-Doniach model.[4,5] It was shown in Ref. 2 that the "lock-in" field $H_{\rm lock\ in}$ is determined by the energy of kink and with logarithmic accuracy is estimated as

$$H_{\rm lock\ in}=\frac{\Phi_0}{4\pi\lambda^2}\left[\ln\left[\frac{\gamma d}{\xi}\right]+C_k\right], \tag{1}$$

here γ is the anisotropy coefficient and λ is the London penetration depth, d is separation between layers. It was argued in Ref. 3 that the indication of the transition should be a kink in the field dependence of the *c* component of the magnetization $M_z(H_z)$ at $H_z=H_{\rm lock\ in}$. The important feature of this dependence is that $-M_z$

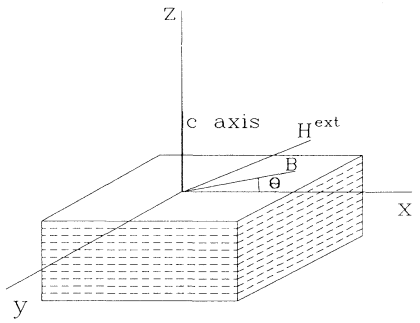

FIG. 1. Layered superconductor in the tilted magnetic field. Choice of the axes.

keeps growing after penetration of H_z^{ext} into the superconductor and reaches a maximum of at some field H_{max} above $H_{lock\ in}$.

In spite of considerable progress a complete description of the transition is still absent because in Refs. 3–5 only the region of high density of kinks has been considered. There a particular structure of the kinked lattice is unimportant and the energy is just determined by the averaged c component of the magnetic induction B_z (i.e., concentration of the kinks). The main purpose of this paper is to consider the structure of the kink lattice and the critical behavior of the magnetization near the "lock-in" transition.

To understand the most favorable configuration of the kink lattice at small concentration of kinks it is important to realize that a single kink cannot exist in the ideal lattice of the Josephson vortices. The reason is that its creation is always accompanied by the creation of linear defect in the lattice, which costs infinite energy [Fig. 2(a)]. This means that at very small densities of kinks they should be collected in separated walls aligned along the yz planes [Fig. 2(b)]. Such a configuration preserves the ideal lattice of Josephson vortices in the regions between the kink walls. The density of the kinks in a single wall is fixed by the density of the Josephson vortices while the separation between the walls L is determined by the z component of the magnetic induction B_z. At large enough L (small B_z) the kink walls can be treated independently. It means that the kink wall rather than a single kink represents the elemental object for field penetration.

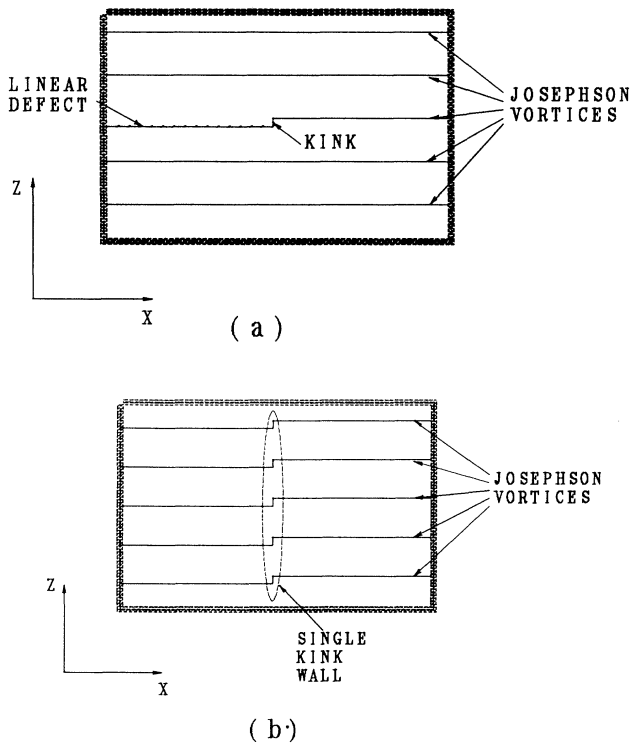

FIG. 2. (a) Single kink in the lattice of Josephson vortices. (b) Single kink wall.

The behavior of the magnetization near the transition is determined by the interaction energy between the kink walls. We will show that at large distances kink walls interact exponentially. This means that the density of the kink walls sharply increases with the internal field H_z in the narrow region above the transition. This leads to a sharp drop of the magnetization. However, kink walls interact exponentially only in the narrow region above the transition. As the exponential interaction breaks down, the magnetization starts to increase again as it was described in Ref. 3. It means that there is a tiny peak in the field dependence of the magnetization M_z near the transition. The amplitude and the width of this peak depend upon the value of the field along the ab planes. There is a typical value of the field B_0 along the layers at which the behavior in the peak region changes significantly, $B_0=\sqrt{3}\Phi_0\gamma/2(2\pi\lambda)^2$. In the high-field region $B_x \gg B_0$ a fast decrease of $-M_z$ breaks down when B_z reaches the typical value $B_{z0}=dB_x/\lambda$. Then a region of weak field dependence of the magnetization follows. The magnetization starts to increase again when B_z reaches another typical field $B_{z1}=(d/\lambda)(B^{3/2}/B_0^{1/2})$. In the low-field region, $B_x < B_0$, a pronounced minimum in the dependence $-M_z(B_z)$ occurs when B_z becomes of the order of B_{z1}.

As was pointed out in Ref. 4, a kink-mediated penetration of H_z^{ext} takes place only if the Josephson coupling between layers is not too weak. The natural measure of the strength of coupling is the anisotropy γ of the London penetration depth. At large enough γ the z component of the field starts to penetrate by means of formation of the Abrikosov flux lines in the direction of the c axis. This leads to the creation of two coexistent lattices of Abrikosov and Josephson vortices ("combined" lattice). The kink-mediated penetration becomes unfavorable when the energy of a kink exceeds the energy of a vortex per unit layer. For exact determination of the critical anisotropy it is important to know the exact value of the numerical constant C_k in Eq. (1). To determine this constant we calculate numerically the energy of kink and obtain $C_k=-0.17$. This gives the following value of the critical anisotropy γ_{cr}:

$$\gamma_{cr}=1.95\lambda/d\ . \tag{2}$$

II. ENERGY OF A KINKED VORTEX LATTICE

We consider a layered superconductor composed of Josephson coupled superconducting planes separated by the distance d. The strength of the coupling can be characterized by the anisotropy ratio γ, $\gamma=\lambda_c/\lambda$, λ_c and λ being the screening lengths for supercurrents flowing along the c axis and along the layers correspondingly. We suppose that inequality $\gamma d < \lambda$ holds. The Lawrence-Doniach model[6] gives the following expression for the energy of a layered superconductor in magnetic field $B \ll B_{c2}$:

$$F(\mathbf{B})=\frac{d}{V}\sum_n \int d^2r \left\{ \frac{\Phi_0^2}{\pi(4\pi\lambda)^2}\left[\nabla\phi_n-\frac{2e}{c}\mathbf{A}\right]^2 + \frac{\Phi_0^2}{\pi(4\pi\lambda_c)^2 d^2}\left[1-\cos\left[\phi_n-\phi_{n-1}-\frac{2e}{c}\int_{z_{n-1}}^{z_n} A_z dz\right]\right]\right\}+\frac{1}{V}\int d^3r\frac{B^2}{8\pi} . \tag{3}$$

The first term in this expression represents the energy of supercurrents in superconducting layers, the second one gives the energy of the Josephson coupling between the layers, and the third one gives the magnetic energy, V is the total volume of superconductor.

We consider the layered superconductor that contains a vortex lattice (i.e., the magnetic induction $\mathbf{B}$) tilted at small angle θ with respect to superconducting ab planes. The choice of the axes is shown in Fig. 1. The lattice is composed of finite pieces of vortex lattice oriented along the layers (see Figs. 3 and 4). Subsequent pieces are separated by the kink walls. Each piece has length L, $L=d/\theta$. The energy of such vortex configuration was estimated in Refs. 2–5 for not too large L. Here we give the expression for the energy valid for large L. The derivation of this expression is given in Appendix A. In the region $B_x>\Phi_0/\lambda\lambda_c$, $\gamma\theta<1$, the result for the kink contribution to the energy, $\delta F(\mathbf{B})=F(B_x,B_z)-F(B_x,0)$, is the following:

$$\delta F(\mathbf{B})=\frac{B_x^2}{8\pi}\left[\frac{d^2}{2L\lambda}\frac{1+\exp(-L/\lambda)}{1-\exp(-L/\lambda)} + \sum_{\mathbf{Q}\neq 0}\frac{\gamma d^2 Q_y^2}{2(\lambda K)^2}G(LK,Q_z)\right]+\frac{B_z}{d\Phi_0}\varepsilon_{nk} , \tag{4}$$

here the sum is performed over the reciprocal-lattice vectors of the triangular lattice, $\mathbf{Q}=(Q_y,Q_z)$, $K(\mathbf{Q})=(\gamma Q_y^2+Q_z^2/\gamma)^{1/2}$, the dimensionless function $G(LK,Q_z)$ is given by

$$G(LK,Q_z)=\frac{2\sinh(LK/\sqrt{\gamma})/(LK/\sqrt{\gamma})}{[2\sinh(LK/2\sqrt{\gamma})]^2+(d\tilde{Q}_z)^2}$$

and has the following asymptotics:

$$G(K,Q_z)=\frac{\sqrt{\gamma}}{LK}\left[1+\cos(dQ_z)\exp\left[-\frac{LK}{\sqrt{\gamma}}\right]\right] \quad \text{at } LK/\sqrt{\gamma}\gg 1 ,$$

$$G(K,Q_z)=\frac{1/L^2}{Q_y^2+(\gamma^{-2}+\theta^2)Q_z^2} \quad \text{at } LK/\sqrt{\gamma}\ll 1 .$$

In the following we consider mainly the situation when nonlinear cores of the Josephson vortices do not overlap, i.e., x component of the induction B_x is smaller than crossover field in parallel direction $B_{cr}^{\parallel}$,[7] $B_x\ll B_{cr}^{\parallel}$, $B_{cr}^{\parallel}=\sqrt{3}\Phi_0/2d^2\gamma$.

At the end of this section we discuss briefly the derivation of magnetization from Eq. (4) and influence of the sample geometry. The dependence of $\mathbf{B}$ on the internal field $\mathbf{H}=\mathbf{B}-4\pi\mathbf{M}$ can be obtained by minimization of the energy $\tilde{F}(\mathbf{H})$,

$$\tilde{F}(\mathbf{H})=F(\mathbf{B})-\frac{\mathbf{H}\cdot\mathbf{B}}{4\pi} \tag{5}$$

with respect to $\mathbf{B}$. It is well known[8] that obtained in such a way dependencies of $\mathbf{H}$ and the magnetization $\mathbf{M}$ on $\mathbf{B}$ are internal properties of the superconducting material while the relation between $\mathbf{H}$, $\mathbf{B}$, and the external field $\mathbf{H}^{\text{ext}}$ depends upon the sample geometry. Experiments are usually performed on thin slabs elongated along the layers. In the field range $H_x^{\text{ext}}\gg\Phi_0/\lambda^2\gamma$ the demagnetizing effects in the parallel direction can be neglected, i.e., $B_x\approx H_x\approx H_x^{\text{ext}}$. On the other hand, at small tilting angle of $\mathbf{H}^{\text{ext}}$ the demagnetizing effects are very strong in the z direction. The standard way to treat this problem is to approximate the shape of the sample by the ellipsoid with the demagnetizing factor $D_z(1-D_z\ll 1)$ for which the fields B_z, H_z, and H_z^{ext} are connected by the exact rela-

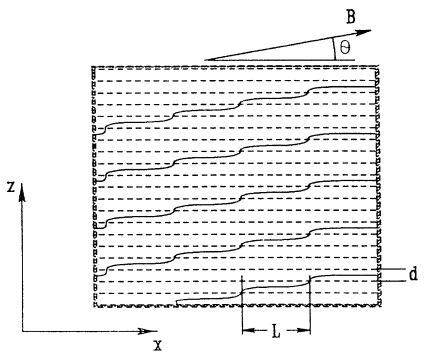

FIG. 3. Kinked vortex lattice.

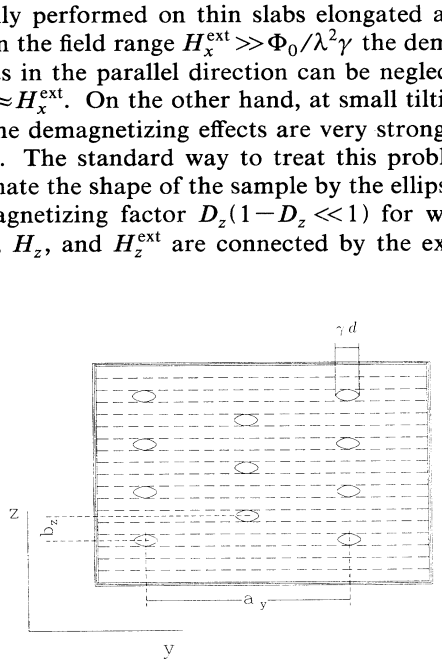

FIG. 4. Stretched lattice of Josephson vortices.

tion[8]

$$(1-D_z)H_z+D_zB_z=H_z^{\rm ext} . \quad (6)$$

III. BOUNDARY OF THE LOCKED PHASE. STRUCTURE OF SINGLE KINK WALL

At small B_z a rarefied lattice of the kink walls is realized and the main contribution to the angular-dependent part of the energy δF arises from energies of separated kink walls

$$\delta F=\sigma_{\rm kw}/L . \quad (7)$$

$\sigma_{\rm kw}$ is the energy of single kink wall per unit area. This energy should be compared with the gain of energy due to the penetration of field, $-B_zH_z/(4\pi)$. Comparison shows that the formation of the kink walls becomes favorable when the internal field exceeds the critical value $H_{\rm lock\ in}$,

$$H_{\rm lock\ in}=\frac{4\pi\sigma_{\rm kw}}{dB_x} . \quad (8)$$

Extracting from Eq. (4) the linear term on $1/L$ we obtain

$$\sigma_{\rm kw}=\frac{B_x^2d^2}{16\pi\lambda}\left[1+\frac{\gamma^{3/2}}{\lambda}\sum_{\mathbf{Q}}\frac{Q_y^2}{[K(\mathbf{Q})]^3}\right]+\frac{B_x}{\Phi_0}\varepsilon_{nk} . \quad (9)$$

This energy can be represented as

$$\sigma_{\rm kw}=\frac{B_x}{\Phi_0}\varepsilon_k+\sigma_{\rm int} . \quad (10)$$

ε_k is the energy of the kink in a single vortex line,[2]

$$\varepsilon_k=\frac{d\Phi_0^2}{(4\pi\lambda)^2}\left[\ln\left[\frac{\gamma d}{\xi}\right]+C_k\right] . \quad (11)$$

This expression is obtained from Eq. (9) as a sum of the second term in the parentheses with changing summation over $\mathbf{Q}$ to integration and the last term. The numerical constant C_k can be obtained by the numerical calculation of the phase distribution induced by a single kink. This calculation is performed in Appendix B. It gives $C_k\approx-0.17$. $\sigma_{\rm int}$ is the kink interaction energy,

$$\sigma_{\rm int}=\begin{cases}\dfrac{B_x^2d^2}{16\pi\lambda}\left[1-\dfrac{C_{\rm int}a_y}{\lambda}\right] & \text{at } B_x<B_{\rm cr}^{\parallel} ,\\ \dfrac{B_x^2d^2}{16\pi\lambda}\left[1-\dfrac{\Phi_0}{\pi d\lambda B_x}\ln\left[\dfrac{a_y}{\gamma d}\right]\right] & \text{at } B_x>B_{\rm cr}^{\parallel}\end{cases} \quad (12)$$

$C_{\rm int}\sim1$. At small magnetic fields, $B_x<B_{\rm cr}^{\parallel}$, the main contribution to $\sigma_{\rm kw}$ comes from the energies of separated kinks.[2,4] This leads to the field-independent "lock-in" field given by Eq. (1). The kink-mediated penetration remains favorable as far as $H_{\rm lock\ in}$ remains smaller than field H_{c1} connected with the penetration of the Abrikosov vortices along the c direction,

$$H_{c1}=\frac{\Phi_0}{4\pi\lambda^2}[\ln(\lambda/\xi)+0.5] .$$

This condition means that the energy of the kink should be smaller than the energy of the Abrikosov vortex per one layer. Comparison shows that the kink-mediated penetration is favorable as the value of the anisotropy is smaller than the critical anisotropy given by Eq. (2).

In the region $B_x>B_{\rm cr}^{\parallel}$, the kink interaction energy becomes comparable with the contribution coming from separated kinks. In this region $H_{\rm lock\ in}$ depends logarithmically upon B_x:

$$H_{\rm lock\ in}=\frac{\Phi_0}{2\pi\lambda^2}\ln\left[\frac{\gamma B_{c2}}{B_x}\right] . \quad (13)$$

As the kink wall represents an elemental object for the field penetration it is interesting to calculate the distribution of field near it. Fourier transform of the z component of the induction is given by

$$B_z(\mathbf{k})=\frac{\Phi_0S_z(\mathbf{k})}{1+\lambda^2k^2} \quad (14)$$

with $S_z(\mathbf{k})=d\sum_j\exp(i\mathbf{k}\cdot\mathbf{R}_j^{(0)}+ik_zd/2)$, $\mathbf{R}_j^{(0)}$ are the positions of the Josephson vortices. The resulting field distribution can be represented as a sum of contributions from the kink chains that form a kink wall (we call a kink chain a row of kinks elongated in the z direction):

$$B_z(x,y)=\frac{\Phi_k}{2\pi\lambda^2}\sum_m K_0\left[\frac{|\rho-\rho_m|}{\lambda}\right] , \quad (15)$$

here $\rho_m=(0,a_ym/2)$ are the chain's coordinates, $\rho=(x,y)$,

$$\Phi_k=\Phi_0\frac{d}{2b_z}=\Phi_0\sqrt{B_x/B_{\rm cr}^{\parallel}} , \quad (16)$$

$K_0(x)$ is a modified Bessel function of zero order. Field distribution near the kink chain occurs to be essentially the same as for the vortex line, however, the value of magnetic flux through the chain Φ_k is smaller than Φ_0. The reason is that the concentration of kinks in the kink chain is smaller than the concentration of the pancake vortices in a vortex line. Periodicity in chain arrangement is determined by periodicity of the Josephson vortex lattice in the y direction. The field distribution depends significantly upon the relation between the field along the layers B_x and the typical magnetic field B_0,

$$B_0=\frac{\sqrt{3}\Phi_0\gamma}{2(2\pi\lambda)^2}=\left[\frac{\gamma d}{2\pi\lambda}\right]^2B_{\rm cr}^{\parallel} . \quad (17)$$

The estimate for this field is

$$B_0=1.1\ {\rm kG}\frac{\gamma/100}{(\lambda/2\times10^{-5}\ {\rm cm})^2} . \quad (18)$$

As field B_x is smaller than B_0 the distance between chains $a_y/2$ is larger than λ and field B_z is concentrated in the well-separated tubes of the radius λ [see Fig. 5(b)]. At high fields $B\gg B_0$ the tubes overlap and the field distribution is represented by the flux wall [Fig. 5(a)]:

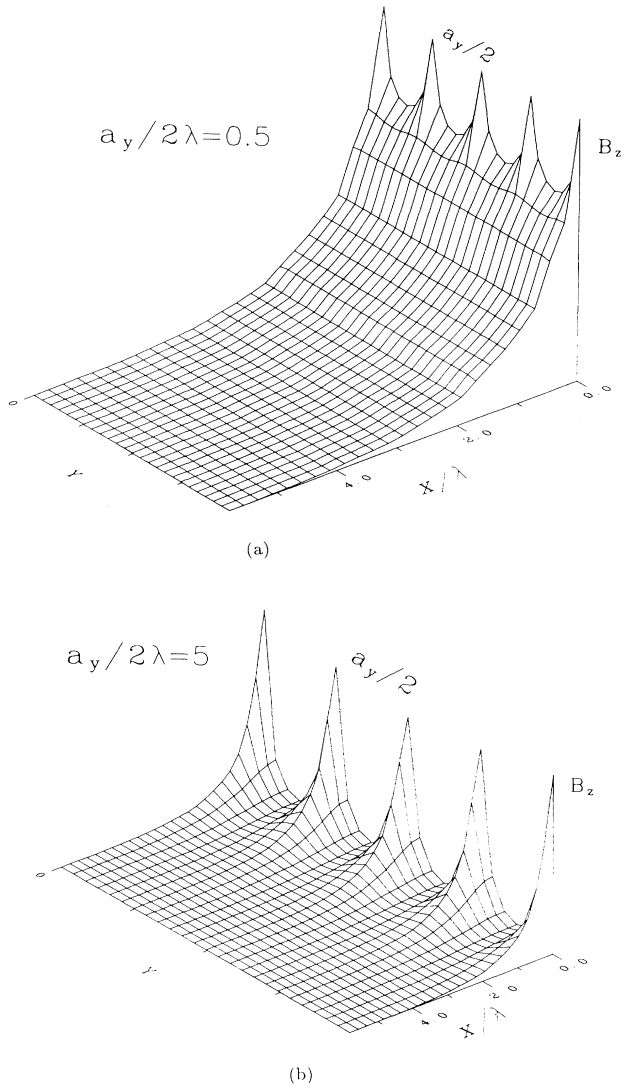

FIG. 5. (a) and (b) Field distribution near the kink wall at different values of B_x.

$$B_z(\rho)\approx\frac{dB}{2\lambda}\left[\exp(-x/\lambda)+\frac{a_y}{2\pi\lambda}\cos(4\pi y/a_y)\exp(-4\pi x/a_y)\right]. \tag{19}$$

Such a structure of the field, in principle, can be observed in the decorations or other imaging experiments.

IV. KINK WALL INTERACTION ENERGY: BEHAVIOR OF THE MAGNETIZATION NEAR THE LOCK-IN TRANSITION

Consider the region close to the lock-in transition, where concentration of the kink walls is small, $L\gg\lambda, a_y$. In this case kink contribution $\delta F(\theta)$ to the lattice energy, $\delta F(\theta)=F(\theta)-F(0)$, can be represented as

$$\delta F(\theta)=\sigma_{\rm kw}/L+E_{\rm int}(L)\ . \tag{20}$$

The behavior near the transition is determined by the interaction energy $E_{\rm int}(L)$ between the kink walls. From Eq. (4) one can obtain

$$E_{\rm int}(L)=\frac{B_x^2d^2}{8\pi\lambda^2}\left[\frac{\lambda}{L}\exp\left[-\frac{L}{\lambda}\right]+\frac{3\sqrt{\gamma}}{LQ_0}\exp\left[-\frac{LQ_0}{\sqrt{\gamma}}\right]\right]. \tag{21}$$

From the latter equation one can see that there are two contributions to the interaction energy. The first term represents interaction mediated by the averaged z component of the magnetic field induced by the kink walls (15). This term coincides with the interaction energy between vortex rows. The second term represents interaction mediated by the oscillating perturbations of the current and field induced by the kink wall. Relation between these terms depends upon the relation between the magnetic induction B and the typical magnetic field B_0. The first term dominates at $B\gg B_0$ and vice versa.

Weak interaction between kink walls leads to fast increase of their concentration as field H_z exceeds the field $H_{\rm lock\ in}$. This leads to the appearance of the sharp peak in the field dependence of the z component of magnetization $M_z(H_z)$. This peak is analogous to the peak in the field dependence of magnetization in isotropic superconductors at the field H_{c1}.[17] However, it has much smaller amplitude and the field dependence of the magnetization above the peak is nonmonotonic. Experiments are usually performed on thin slabs, which have z components of the demagnetizing factor D_z close to one. For such samples above the transition z component of the magnetic induction B_z is connected with the z component of the external field $H_z^{\rm ext}$ by the simple relation $B_z\approx H_z^{\rm ext}-(1-D_z)H_{\rm lock\ in}$. It means that the dependence $M_z(B_z)$ rather than $M_z(H_z)$ can be directly extracted from the experiment. The behavior of M_z can be easily obtained from Eq. (21):

$$4\pi M_z(B_z)=4\pi M_z(0)+B_z-\frac{B_{z0}^2}{2B_z}\left[\exp\left[-\frac{B_{z0}}{B_z}\right]+3\exp\left[-\frac{B_{z1}}{B_z}\right]\right]. \tag{22}$$

Here $M_z(0)=-H_{\rm lock\ in}/4\pi$ is the value of the magnetization at the transition,

$$B_{z0}=B_xd/\lambda\ ,\qquad B_{z1}=B_{z0}(B_x/B_0)^{1/2}\ . \tag{23}$$

The exponential interaction between kink walls breaks down when the z component of the magnetic induction reaches the smallest of the fields B_{z0}, B_{z1}, i.e., distance L

between the kink wall equalizes with smallest of the lengths λ and $a_y/2$. Two types of behavior above the peak are possible depending upon the ratio of the induction B and the field B_0 (i.e., upon the ratio of B_{z1} and B_{z0}). Consider the region $B > B_0$ ($B_{z1} > B_{z0}$). In this region exponential interaction between kink walls breaks down when B_z exceeds B_{z0}. From Eq. (4) it is possible to obtain the expression for lattice energy valid in the whole region $B_z < B_{z1}$:

$$\delta F = \frac{H_{\text{lock in}} B_z}{4\pi} + \frac{B_z B_{z0}/8\pi}{\exp(B_{z0}/B_z)-1} + \frac{3B_{z0}^2 B_z}{8\pi B_{z1}} \exp\left[-\frac{B_{z1}}{B_z}\right] . \quad (24)$$

Field dependence of the magnetization in this region is given by

$$4\pi M_z(B_z) = 4\pi M_z(0) + B_z - \frac{B_{z0}}{2}\left[\frac{\exp(B_{z0}/B_z)(1+B_{z0}/B_z)-1}{[\exp(B_{z0}/B_z)-1]^2} + \frac{3B_{z0}}{B_z}\exp\left[-\frac{B_{z1}}{B_z}\right]\right] . \quad (25)$$

It follows from the latter expression that the field dependence of M_z has plateau in the field range $B_{z0} < B_z < B_{z1}$. The magnetization in the plateau region is given by $4\pi M(B_z) - 4\pi M(0) = B_{z0}/4$. $-M_z(B_z)$ starts to increase again when the field reaches B_{z1}. The field $B_z^{\min}$ where minimum of $-M_z(B_z)$ occurs can be obtained from the relation

$$B_z^{\min} = B_{z1} / \ln\left[\frac{360 B_{z1} B_z^{\min}}{B_{z0}^2}\right] . \quad (26)$$

In the region $B_z > B_{z0}, B_{z1}$ but $B_z < B_x/\gamma$, the magnetization increases almost linearly:

$$-M_z(B_z) = -M_z(0) + \frac{B_0 B_z}{4\sqrt{3} B_x}\left[\ln\frac{B}{B_{z1}} + 0.16\right] . \quad (27)$$

The maximum of $-M_z(B_z)$ occurs at $B_z \geq B_x/\gamma$.[3] It is noteworthy that the behavior of $-M_z(B_z)+M_z(0)$ near the transition [Eqs. (22), (25), and (27)] is determined by wave vectors $k_z \gg \pi/d$ and therefore is not influenced by the nonlinear Josephson contribution to the lattice energy.

Crossover between the regions $B_x < B_{z1}$ and $B_x > B_{z1}$ can be obtained only numerically. A series of the numerically calculated curves $-M(B_z)+M(0)$ at different values of B_x is represented in Fig. 6.

V. CONCLUSIONS

We studied in detail the behavior of layered superconductors in a tilted magnetic field at small values of the z component of the magnetic induction. We argue that penetration of this component occurs by means of the formation of kink walls. The distribution of the magnetic field near the wall and the behavior of the magnetization depend upon ratio of the field along the layers and the typical field B_0 [Eq. (17)].

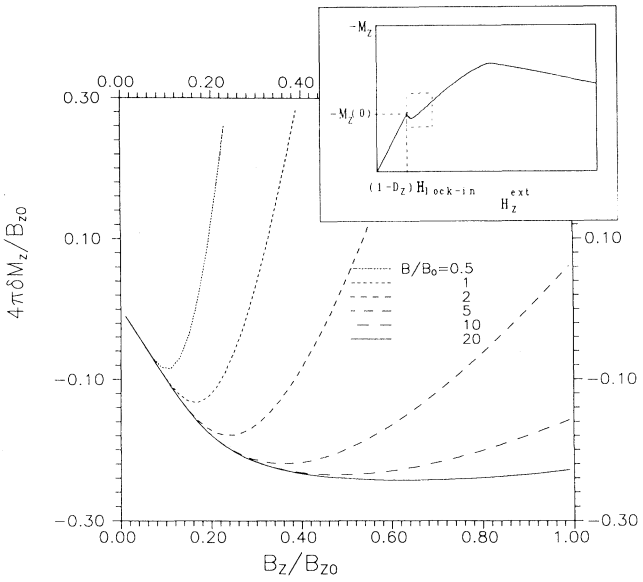

FIG. 6. Dependencies of the magnetization $\delta M_z = M_z(0) - M_z$ upon the magnetic induction B_z near the lock-in transition at different values of B_x. The inset shows a schematic field dependence of the magnetization in the z direction in a large field scale. The box restricts the region represented in the main figure.

A schematic phase diagram at low angles is represented in Fig. 7. At fixed B_x the low-angle behavior is characterized by *three* typical fields along the c axis $B_{z0}(B_x)$, $B_{z1}(B_x)$, and B_x/γ [see Eqs. (23)]. In the region $B_z < B_{z0}, B_{z1}$ layered structure of superconductor influences essentially on both structures of individual vortices and intervortex interaction. This region corresponds to exponentially weak interacting kink walls and sharp decrease of magnetization with H_z. In the region $B_{z0}, B_{z1} < B_z < B_x/\gamma$ vortices preserve their kinked struc-

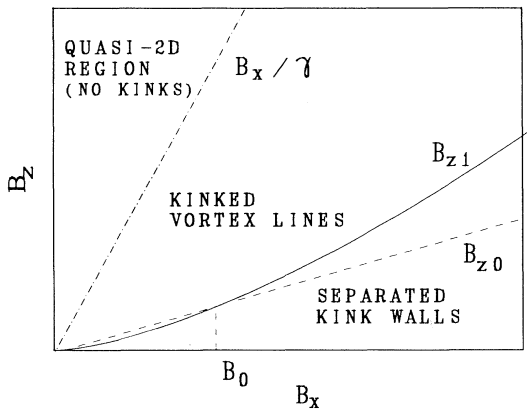

FIG. 7. Schematic phase diagram at low angles.

ture but the intervortex interaction energy coincides with one given by anisotropic Ginzburg-Landau theory. This region corresponds to almost linear increase of the magnetization. In the region $B_z \sim B_x/\gamma$ the layered structure influences weakly on the behavior of the superconductor.

The most natural way to detect the lock-in transition is to perform precise measurements of magnetization or torque at small tilting angles of the external field (in highly anisotropic superconductors the torque gives the component of the magnetization along the c axis). The "fingerprint" of the transition is a tiny peak in the field dependence of the magnetization, which is followed by its further increase. However, in published papers devoted to the precise angular measurements of the magnetization[9,10] in $Bi_2Sr_2CaCu_2O_7$ (BSCCO), and the torque[11–13] (BSCCO),[14] ($Tl_2Ba_2CaCu_2O_7$) these features were not observed. There are several possible explanations for this. First, the tiny peak above the transition exists in a very narrow range $\delta\theta$ of the tilting angles of $\mathbf{B}$, $\delta\theta \leq d/\lambda$. For BSCCO ($d=1.5\times10^{-7}$ cm, $\lambda\approx3\times10^{-5}$ cm at $T=77$ K) this gives $\delta\theta \leq 0.3°$. This means that the peak can be observed only in very precise measurements performed on high-quality single crystals. Usually the low-angle intrinsic behavior is smeared out by misorientation of the c axis. Second, recent torque measurements performed on high-quality single crystals[12,13] show that the value of anisotropy in BSCCO is much larger than it was reported earlier[11] and it may be quite possible that in the considerable temperature range the value of anisotropy γ is larger than the temperature-dependent critical anisotropy γ_{cr} given by Eq. (2) (for BSCCO at $T=77$ K the critical anisotropy can be estimated as $\gamma_{cr}\approx400$). In this case penetration of H_z^{ext} should occur by means of formation of the Abrikosov vortices.[4] Third, the transition seems to be observable in a limited temperature range because at high temperatures it is destroyed by thermal fluctuations while at low temperatures it is smeared out by the pinning potential. For BSCCO the temperature range within which observation of the lock-in transition can be expected at $B<1$ T can be estimated as 50–70 K.

ACKNOWLEDGMENTS

I would like to thank P. H. Kes, J. C. Martinez, L. N. Bulaevskii, and J. Aarts for useful discussions. This work was supported by the Netherlands Foundation for the Fundamental Research of Matter (Stichting FOM).

APPENDIX A: DERIVATION OF THE EXPRESSION FOR THE KINK CONTRIBUTION TO THE LATTICE ENERGY [Eq. (4)]

With logarithmic accuracy the energy of the vortex configuration can be obtained within linear approximation, i.e., by expanding the cosine term in Eq. (3) with respect the gauge-invariant phase difference. This approximation breaks down at distances $\sim\gamma d$ from the cores of the Josephson vortices. Within the linear approximation the energy can be calculated exactly with use of the Fourier transform.[2,4] The exact expression for the energy can be represented as a sum of linear and nonlinear contributions:

$$F(\mathbf{B})=\frac{\Phi_0^2}{8\pi V}\int\frac{d^3k}{(2\pi)^3}\left[\frac{|S_x|^2+[(1+\lambda_c^2k^2)/(1+\lambda^2k^2)]|S_z|^2}{1+\lambda^2\tilde{k}_z^2+\lambda_c^2k_\perp^2}\right]+F_{nl}(\mathbf{B})\ . \tag{A1}$$

Here $\tilde{k}_z=(2/d)\sin(dk_z/2)$, $|k_z|\leq\pi/d$, $k_\perp^2=k_x^2+k_y^2$, $k^2=\tilde{k}_z^2+k_\perp^2$,

$$\mathbf{S}(\mathbf{k})=\sum_j\int dx\frac{d\mathbf{R}_j}{dx}\exp[i\mathbf{k}\cdot\mathbf{R}_j(x)]\ ,$$

$\mathbf{R}_j(x)=[x,Y_j,Z_j,(x)]$ are the coordinates of the vortex lines (Fig. 3). Each vortex line is composed of the portions of Josephson vortices separated by kinks (Fig. 3). The first term in Eq. (A1) represents a linear contribution to the energy, while $F_{nl}(\mathbf{B})$ gives the nonlinear Josephson contribution. In the region $\gamma\theta<1$ the latter contribution can be represented as

$$F_{nl}(\mathbf{B})=\frac{B_x}{\Phi_0}\epsilon_{nJ}+\frac{B_z}{d\Phi_0}\varepsilon_{nk}\ .$$

Here ϵ_{nJ} and ε_{nk} are the nonlinear Josephson contributions to the line energy of a Josephson vortex and to the energy of a kink correspondingly, $\epsilon_{nJ}=\alpha_J\Phi_0^2/(4\pi)^2\lambda\lambda_c$, $\varepsilon_{nk}=\alpha_k d\Phi_0^2/(4\pi\lambda)^2$. The numerical constants α_J and α_k can be estimated from the energies of a Josephson vortex and a kink, which are numerically calculated in Appendix B, $\alpha_J\approx-0.53$, $\alpha_k\approx0.33$. Nonlinear contribution from the normal cores of the kinks can be taken into account by the right choice of the upper cutoff in the integration over $k_\perp$, $k_\perp<1.65/\xi$.

For the kinked vortex lattice (see Fig. 3) $Z_j(x)$ are given by $Z_j(x)=Z_j^{(0)}+nd$ at $(n-\frac{1}{2})L<x<(n+\frac{1}{2})L$ and the components of the vector $\mathbf{S}$ are reduced to

$$\begin{aligned}S_x&=\frac{\sin(k_xL/2)}{(k_x/2)}\sum_{j,n}\exp[i\mathbf{k}\cdot\mathbf{R}_j^{(0)}+i(k_zd+k_xL)n]\ ,\\ S_z&=d\sum_{j,n}\exp[i\mathbf{k}\cdot\mathbf{R}_j^{(0)}+i(k_zd+k_xL)(n+\tfrac{1}{2})]\ .\end{aligned} \tag{A2}$$

The separation between the kink walls L is connected with the tilting angle θ of the field with respect to ab planes by the simple relation $L=d/\theta$, i.e., the z component of the magnetic induction is given by $B_z=B_xd/L$.

Summation over index j corresponds to summation over the sites $\mathbf{R}_j^{(0)}=(Y_j^{(0)},Z_j^{(0)})$ of the triangular lattice of the Josephson vortices which is stretched along the y axis

(see Fig. 4),

$$Y_j^{(0)}=(j_1+\tfrac{1}{2}j_2)a_y \ ,$$

$$Z_j^{(0)}=j_2 b_z \ ,$$

$a_y=a\sqrt{\gamma}$, $b_z=(\sqrt{3}/2)a/\sqrt{\gamma}$, $a=(2\Phi_0/\sqrt{3}B)^{1/2}$ is the averaged parameter of the vortex lattice. In the region $\gamma\theta<1$ one can neglect the change with B_z of the lattice parameters a_y and b_z.

Substituting Eqs. (A2) into Eq. (A1) we obtain a useful intermediate result:

$$F(\mathbf{B})=\frac{B_x\Phi_0}{8\pi}L\sum_{j,n}\int\frac{d^3k}{(2\pi)^3}\exp[i\mathbf{k}\cdot\mathbf{R}_j^{(0)}+i(k_xL+dk_z)n]\frac{[(1+\lambda_c^2k^2)/(1+\lambda^2k^2)]\theta^2+\sin^2(k_xL/2)/(k_xL/2)^2}{1+\lambda^2\tilde{k}_z^2+\lambda_c^2k_\perp^2}+F_{\rm nl} \ . \tag{A3}$$

Using the identity $\sum_j\exp(i\mathbf{k}\cdot\mathbf{R}_j^{(0)})=(B/\Phi_0)\sum_{\mathbf{Q}}\delta(\mathbf{k}-\mathbf{Q})$, where $\mathbf{Q}$ are the reciprocal-lattice vectors

$$Q_y=\frac{\sqrt{3}}{2}m_2Q_0/\sqrt{\gamma} \ ,$$

$$Q_z=(m_1+\tfrac{1}{2}m_2)Q_0\sqrt{\gamma} \ ,$$

$Q_0=2\pi(2B/\sqrt{3}\Phi_0)^{1/2}$, and performing integration over k_x, we finally obtain the following expression for lattice energy in the range $B>\Phi_0/\lambda\lambda_c$, $\gamma\theta<1$:

$$F(\mathbf{B})=F_J(B_x)+\delta F(\mathbf{B}) \ . \tag{A4}$$

Here

$$F_J(\mathbf{B})=\frac{B_x^2}{8\pi}\left[1+\sum_{\mathbf{Q}\neq0}\frac{1}{\gamma[\lambda K(\mathbf{Q})]^2}\right]+\frac{B_x}{\Phi_0}\epsilon_{\rm nJ} \tag{A5}$$

is the energy of the lattice of the Josephson vortices, the kink contribution to the energy, $\delta F(\mathbf{B})=F(B_x,B_z)-F(B_x,0)$, is given by Eq. (4).

APPENDIX B: NUMERICAL CONSTANTS FOR VORTICES IN LAYERED SUPERCONDUCTORS

1. Energy of a Josephson vortex

The energy of a Josephson vortex in the layered superconductor is determined by the minimum of the functional

$$\epsilon=\frac{d\Phi_0^2}{\pi(4\pi\lambda)^2}\sum_n\int dy\left\{\frac{1}{2}\left[\frac{d\phi_n}{dy}-\frac{2\pi}{\Phi_0}A_y\right]^2+\frac{1}{(\gamma d)^2}\left[1-\cos\left[\phi_{n+1}-\phi_n-\frac{2\pi d}{\Phi_0}A_z\right]\right]\right\}+\int\int dy\,dz\frac{B_x^2}{8\pi} \tag{B1}$$

with respect to the phases $\phi_n(y)$ and the vector potential $\mathbf{A}(y,z)$ under the conditions

$$\phi_1-\phi_0\to\begin{cases}0 & \text{at } y\to\infty \ ,\\ 2\pi & \text{at } y\to-\infty \ ,\end{cases} \tag{B2}$$

with logarithmic accuracy the energy of the Josephson vortex is given by[15]

$$\epsilon_J=\frac{\Phi_0^2}{(4\pi\lambda)^2\gamma}[\ln(\lambda/d)+C_J] \ . \tag{B3}$$

Here we give the estimate for the numerical constant C_J. The same problem has been considered in a recent paper of Clem, Coffey, and Hao.[16] However, we find that the trial phase distribution used in this paper yielding $C_J\approx1.12$ is not sufficiently accurate. Below we represent a variational solution that gives a better approximation to the exact phase distribution and give the corrected value of C_J.

After introducing dimensionless variables

$$\tilde{y}=y/(\gamma d) \ ,$$

$$\tilde{z}=z/d \ ,$$

$$a_y=2\pi\gamma d\,A_y/\Phi_0 \ , \tag{B4}$$

$$a_z=2\pi d\,A_z/\Phi_0 \ ,$$

the energy can be represented as

$$\epsilon=\frac{\Phi_0^2}{\pi(4\pi\lambda)^2\gamma}\tilde{\epsilon} \tag{B5}$$

with

$$\tilde{\epsilon}=\sum_n\int d\tilde{y}\left[\frac{1}{2}\left[\frac{d\phi_n}{d\tilde{y}}-a_y\right]^2+1-\cos(\phi_{n+1}-\phi_n-a_z)\right]+\frac{\lambda^2}{2d^2}\int d^2\tilde{r}\,b_x^2 \ . \tag{B6}$$

To estimate the constant C_J in Eq. (B3) we use the method of the intermediate scale. We chose the dimensionless distance r_0 within interval $1 \ll r_0 \ll \lambda/d$ and the energy $\tilde{\epsilon}$ is represented as a sum of contributions from the regions $\tilde{r} > r_0$ and $\tilde{r} < r_0$, $\tilde{\epsilon} = \tilde{\epsilon}_1 + \tilde{\epsilon}_2$. In the region $\tilde{r} > r_0$ both nonlinearity and discreteness can be neglected because they give an error of order d/r_0. The contribution to $\tilde{\epsilon}$ from this region is the same as for Abrikosov vortices[17] and is estimated as

$$\tilde{\epsilon}_1 = \pi K_0(dr_0/\lambda) \approx \pi[\ln(\lambda/dr_0) + 0.116] . \tag{B7}$$

On the other hand, in the region $\tilde{r} < r_0$, screening (i.e., the vector potential **a**) can be neglected. This gives a mistake of the order of $(r_0/\lambda)^2$. Contribution to the energy from this region is given by

$$\tilde{\epsilon}_2 = \pi[\ln(r_0) + C_2] . \tag{B8}$$

Hence,

$$C_J = C_2 + 0.116 . \tag{B9}$$

An estimate of the constant C_2 is the most difficult part of the problem because it is determined by the phase distribution $\phi_n^{(J)}(\tilde{y})$ in the nonlinear core of the vortex. The latter is given by the solution of the set of nonlinear differential equations

$$\frac{d^2\phi_n^{(J)}}{d\tilde{y}^2} + \sin(\phi_{n+1}^{(J)} - \phi_n^{(J)}) + \sin(\phi_{n-1}^{(J)} - \phi_n^{(J)}) = 0 \tag{B10}$$

under the conditions analogous to (B2). Because of symmetry properties of the solution it is enough to find $\phi_n(\tilde{y})$ in the region $n \geq 1$, $y \geq 0$. The constant C_2 is determined by the minimum value of the functional $C[\phi_n(\tilde{y})]$,

$$C[\phi_n(\tilde{y})] = \frac{4}{\pi} \sum_{n=1}^{N} \int_0^{y_n} d\tilde{y} \left[\frac{1}{2} \left(\frac{d\phi_n}{d\tilde{y}} \right)^2 + 1 - \cos(\phi_{n+1} - \phi_n) \right] - \frac{2}{\pi}[1 - \cos(\phi_1 - \phi_0)] - \ln(N) ,$$
$$y_n = [N^2 - (n - \tfrac{1}{2})^2]^{1/2} \tag{B11}$$

under the conditions $\phi_n(0) = \pi/2$, $\phi_0(y) = -\phi_1(y)$. We chose the scale r_0 to be equal to the integer number N. We find the phase distribution in two steps. First, we find the approximation for $\phi_n(\tilde{y})$ using the variational approach. As a variational ansatz we use the expansion in the solutions of the two-dimensional Laplace equation cut at small distances:

$$\phi_n^{(v)}(\tilde{y}) = \tilde{\theta} + \frac{a_1}{2} \frac{\sin(2\tilde{\theta})}{\tilde{r}^2 + a_2^2} + \frac{b_1}{2} \frac{\sin(2\tilde{\theta})[\cos(2\tilde{\theta}) + b_3]}{(\tilde{r}^2 + b_2^2)^2} \tag{B12}$$

with $\tilde{\theta} = \tan^{-1}[(n - \frac{1}{2})/\tilde{y}]$, $\tilde{r} = \sqrt{(n - 1/2)^2 + \tilde{y}^2}$. Numerical minimization of $C[\phi_n(\tilde{y})]$ for $N = 15$ with respect to the five constants $a_{1,2}$, $b_{1,2,3}$ gives

$$a_1 = 0.350 ,$$
$$a_2 = 0.615 ,$$
$$b_1 = 8.806 ,$$
$$b_2 = 1.420 ,$$
$$b_3 = -2.775 ,$$

and

$$C_2 = 1.43 . \tag{B13}$$

Expression (B12) gives a better approximation to the exact phase distribution than the one used in Ref. 16. This can be checked by direct substitution of both expressions into Eq. (B10).

On the second step the difference $\delta\phi_n(\tilde{y})$ between the exact solution $\phi_n^{(J)}(\tilde{y})$ and the variational approximation $\phi_n^{(v)}(\tilde{y})$, $\delta\phi_n(\tilde{y}) = \phi_n^{(J)}(\tilde{y}) - \phi_n^{(v)}(\tilde{y})$, was found by numerical solution of the relaxation equation:

$$\frac{\partial\delta\phi_n}{\partial t} = \frac{\partial^2\phi_n^{(v)}}{\partial\tilde{y}^2} + \frac{\partial^2\delta\phi_n}{\partial\tilde{y}^2} + \sin(\phi_{n+1}^{(v)} - \phi_n^{(v)} + \delta\phi_{n+1} - \delta\phi_n) + \sin(\phi_{n-1}^{(v)} - \phi_n^{(v)} + \delta\phi_{n-1} - \delta\phi_n) \tag{B14}$$

within the interval $1 \leq n \leq 6$, $\tilde{y} < 5$. The correction $\delta\phi_n(\tilde{y})$ is obtained as a limit of the solution of Eq. (B14) at large t. The obtained deviation $\delta\phi_n(\tilde{y})$ never exceeds 1.5×10^{-2}. This confirms that expression (B12) gives a good approximation to the exact solution. The obtained phase distributions $\phi_n^{(J)}(\tilde{y})$ are plotted in Fig. 8 together with their variational approximations. The correction to C_2 induced by $\delta\phi_n(\tilde{y})$ occurs to be only in the fourth significant digit.

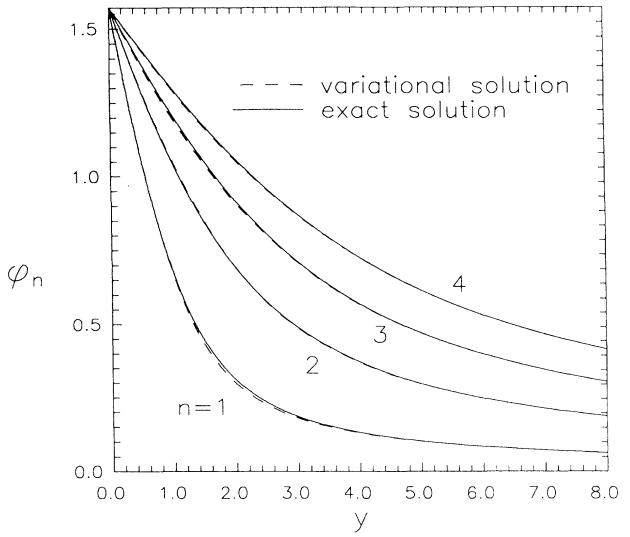

FIG. 8. Phase distributions in the core of a Josephson vortex for the four first layers. Dashed lines represent the variational solution given by Eq. (B12). Solid lines represent the exact phase distribution obtained by the numerical solution of Eq. (B10).

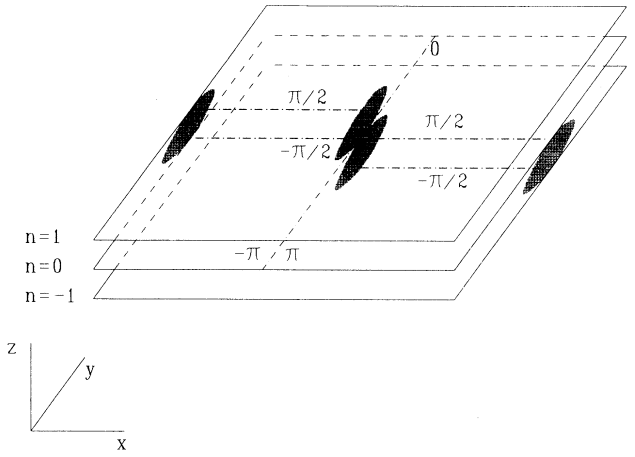

FIG. 9. Kink on the Josephson vortex.

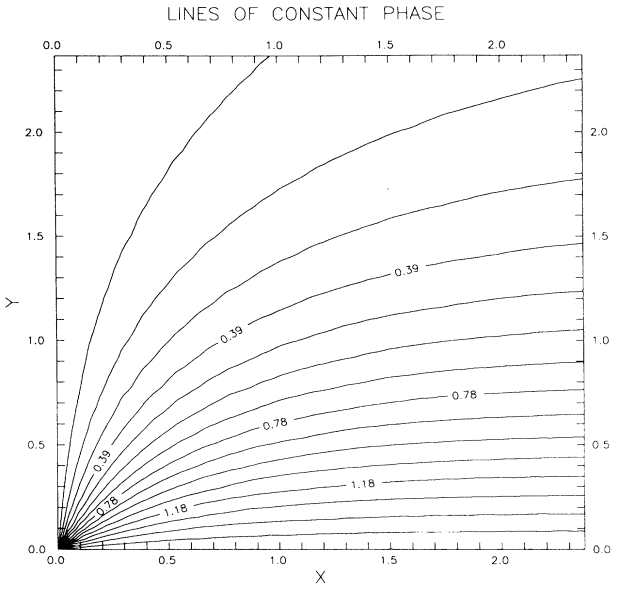

FIG. 10. Lines of the constant phase in the central layer of a kink: the x and y axes correspond to $\phi_0^{(k)}=\pi/2$ and 0, respectively. The lines of the current are directed perpendicular to these lines.

Finally, using Eqs. (B5), (B7), (B8), (B9), and (B13) we obtain for the energy for the Josephson vortex

$$\epsilon=\frac{\Phi_0^2}{(4\pi\lambda)^2\gamma}\left[\ln\left[\frac{\lambda}{d}\right]+1.55\right] . \tag{B15}$$

The constant $C_J=1.55$ should be compared with the value 1.12 given in the Ref. 16.

Using the exact phase distribution we can also estimate other parameters characterizing the properties of the Josephson vortex. The maximum supercurrent, flowing in the superconducting planes, $j_{\max}$, is estimated as

$$j_{\max}=\frac{c\Phi_0}{8\pi^2\lambda^2\gamma d}\frac{d\phi_1^{(J)}}{d\tilde{y}}(\tilde{y}=0) . \tag{B16}$$

Numerically calculated solution gives

$$(d\phi_1^{(J)}/d\tilde{y})(\tilde{y}=0)\approx 1.105$$

and the maximum current can be represented as

$$j_{\max}=2.87\frac{\xi}{\gamma d}j_s , \tag{B17}$$

here $j_s=c\Phi_0/12\sqrt{3}\pi^2\lambda^2\xi$ is the depairing current.[17]

Maximum Josephson current between the central layers of the vortex flows at the distance

$$r_{\max}=0.826\gamma d \tag{B18}$$

from the position of the core.

2. Energy of a kink

The kink separates two parts of a Josephson vortex shifted in the z direction by one interlayer spacing (see Fig. 9). We consider the kink located at the point $\mathbf{r}_\perp=0$ of the plane $n=0$. It means that the phase distribution for the kinked vortex $\phi_n^{(k)}(\mathbf{r}_\perp)$ has the following asymptotics:

$$\phi_n^{(k)}(\mathbf{r}_\perp)\rightarrow\begin{cases}\phi_{n+1}^{(J)}(y) & \text{at } x\gg\gamma d ,\\ \phi_n^{(J)}(y) & \text{at } x\ll-\gamma d .\end{cases} \tag{B19}$$

Here $\phi_n^{(J)}(y)$ is the phase distribution for a Josephson vortex found in the previous section. On the other hand, at small distances in the plane $n=0$ the phase distribution is essentially the same as for an Abrikosov vortex

$$\phi_0^{(k)}(\mathbf{r}_\perp)\approx\tan^{-1}(x/y) \quad \text{at } x\ll\gamma d . \tag{B20}$$

The kink energy is determined by distances $r\sim\gamma d$ and planes with $|n|\sim 1$. On the other hand, screening of the supercurrent becomes important at distances $r\sim\gamma\lambda$ and $n\sim\lambda/d$. It means that the contribution to the energy caused by perturbations of the vector potential can be neglected. Hence, the energy is given by the minimum value of the functional $E_k[\phi_n(\mathbf{r}_\perp)]$,

$$E_k[\phi_n(\mathbf{r}_\perp)]=\frac{d\Phi_0^2}{\pi(4\pi\lambda)^2}\sum_n\int_{\substack{|x|<L\\ r>c_0\xi}}d\mathbf{r}_\perp\left[\frac{1}{2}\left[\frac{d\phi_n}{d\mathbf{r}_\perp}\right]^2+\frac{1}{(\gamma d)^2}[1-\cos(\phi_{n+1}-\phi_n)]\right]-2L\epsilon_J \tag{B21}$$

under conditions (B19). The constant c_0 in the cutting distance at small scales should be the same as for the Abrikosov vortex. The latter can be estimated from the energy of an Abrikosov vortex[18,19]

$$\epsilon_A=\frac{\Phi_0^2}{(4\pi\lambda)^2}[\ln(\lambda/\xi)+0.5]\ . \tag{B22}$$

This estimate gives $c_0\approx 0.68$.

The main contribution to the energy of the kink comes from the kinetic energy of supercurrents flowing in the plane $n=0$ in the region $\xi\ll r\ll\gamma d$. With logarithmic accuracy the energy of the kink is given by[2,4]

$$\epsilon_k=\frac{d\Phi_0^2}{(4\pi\lambda)^2}\left[\ln\left[\frac{\gamma d}{\xi}\right]+C_k\right]\ . \tag{B23}$$

Here we give the estimate for the numerical constant C_k.

After introducing dimensionless variables (B4) and $\tilde{x}=x/(\gamma d)$, the constant C_k can be determined as a minimum value of the functional $C[\phi_n(\mathbf{r}_\perp)]$,

$$C[\phi_n(\mathbf{r}_\perp)]=\frac{1}{\pi}\sum_n\int_{\substack{|\tilde{x}|<\tilde{L}\\ r>r_{\min}}}d\tilde{\mathbf{r}}_\perp\left[\frac{1}{2}\left[\frac{d\phi_n}{d\tilde{\mathbf{r}}_\perp}\right]^2+1-\cos(\phi_{n+1}-\phi_n)\right]-2\tilde{L}\tilde{\epsilon}_J-\ln(c_0/r_{\min}) \tag{B24}$$

with $r_{\min}\ll 1$. The phase distribution $\phi_n^{(k)}(\mathbf{r}_\perp)$ which gives the minimum to this functional obeys the set of nonlinear equations

$$\Delta\phi_n^{(k)}+\sin(\phi_{n+1}^{(k)}-\phi_n^{(k)})+\sin(\phi_{n-1}^{(k)}-\phi_n^{(k)})=0\ . \tag{B25}$$

In the region $\tilde{x},\tilde{y}\gg 1$, Eq. (B25) reduces to a 3D Laplace equation and the asymptotics of $\phi_n^{(k)}(\tilde{\mathbf{r}}_\perp)$ in this region can be found exactly:

$$\phi_n^{(k)}(\mathbf{r}_\perp)=\frac{1}{2}\left[\frac{\tilde{x}}{\tilde{r}}+1\right]\phi_{n+1}^{(J)}(\tilde{y})+\frac{1}{2}\left[\frac{\tilde{x}}{\tilde{r}}-1\right]\phi_n^{(J)}(\tilde{y})\ , \tag{B26}$$

$$\tilde{r}=\sqrt{\tilde{x}^2+\tilde{y}^2+n^2}\ .$$

To find the phase distribution we use the same scheme as for the Josephson vortex. First, we find a rude approximation for $\phi_n^{(k)}(\tilde{\mathbf{r}}_\perp)$ with use of the variational approach. As a variational ansatz we use the function $\phi_n^{(\mathrm{var})}(\tilde{\mathbf{r}}_\perp)$,

$$\begin{aligned}\phi_n^{(\mathrm{var})}(\tilde{\mathbf{r}}_\perp)&=\phi_{n+1}^{(J)}(\tilde{y})+\tfrac{1}{2}[\phi_{n+1}^{(J)}(\tilde{y})-\phi_n^{(J)}(\tilde{y})]\left[\frac{\tilde{x}}{\sqrt{\tilde{r}_\perp^2+(n+b)^2}}-1\right]\ \text{at } n\neq 0\ ,\\ \phi_0^{(\mathrm{var})}(\tilde{\mathbf{r}}_\perp)&=\phi_1^{(J)}(\tilde{y})+\frac{1}{2}\frac{\phi_1^{(J)}(\tilde{y})-\phi_0^{(J)}(\tilde{y})}{a+\tilde{y}^2}\left[\frac{2a}{\pi}\tan^{-1}(\tilde{y}/\tilde{x})+\tilde{y}^2\left[\frac{\tilde{x}}{\sqrt{\tilde{r}_\perp^2+b^2}}-1\right]\right]\ .\end{aligned} \tag{B27}$$

Substitution of (B27) into Eq. (B24) and numerical minimization with respect to the variational parameters a and b gives

$$a=0.057,\quad b=0.10\ ,$$

and

$$C_k^{(\mathrm{var})}=-0.10\ .$$

On the second stage we solve numerically Eq. (B25) by the relaxation method (see previous section) using the variational solution (B27) as the initial approximation. The numerical solution was performed within the interval $0<\tilde{x},\ \tilde{y}<3,\ -2<n<2$. To visualize the solution we present in Fig. 10 the lines of the constant phase for the central plane $n=0$, $\phi_0^{(k)}(\tilde{x},\tilde{y})=\mathrm{const}$. Numerical integration of (B24) with the obtained solution gives

$$C_k=-0.17\ . \tag{B28}$$

*Permanent address: Institute of Solid State Physics, Chernogolovka, 142432 Moscow Region, Russia.

[1]D. Feinberg and C. Villard, Phys. Rev. Lett. **65**, 919 (1990); Mod. Phys. Lett. B **4**, 9 (1990).

[2]B. I. Ivlev, Y. N. Ovchinnikov, and V. L. Pokrovskii, Mod. Phys. Lett. **5**, 73 (1991).

[3]S. S. Maslov and V. L. Pokrovskii, Europhys. Lett. **14**, 591 (1991); Pis'ma Zh. Eksp. Teor. Fiz. **53**, 614 (1991).

[4]L. N. Bulaevskii, M. Ledvij, and V. G. Kogan, Phys. Rev. B **46**, 366 (1992).

[5]D. Feinberg, Physica C **194**, 126 (1992).

[6]W. E. Lawrence and S. Doniach, in *Proceedings of the 12th International Conference on Low Temperature Physics, Kyoto, Japan, 1970,* edited by E. Kanda (Keigaku, Tokyo, 1971), p. 361.

[7]K. B. Efetov, Zh. Eksp. Teor. Fiz. **76**, 1781 (1979) [Sov. Phys. JETP **49**, 905 (1979)].

[8]L. D. Landau and E. M. Lifshitz, *Electrodynamics of the Con-*

tinuum Media (Pergamon, Oxford, 1983).
[9]M. Tuominen, A. M. Goldman, Y. M. Chang, and P. Z. Jiang, Phys. Rev. B **42**, 412 (1990).
[10]N. V. Zavaritsky and V. N. Zavaritsky, Pis'ma Zh. Eksp. Teor. Fiz. **53**, 212 (1991) [JETP Lett. **53**, 226 (1991)].
[11]D. E. Farrell, S. Bonham, J. Foster, Y. C. Chang, P. Z. Jiang, K. G. Vandervoort, D. L. Lam, and V. G. Kogan, Phys. Rev. Lett. **63**, 782 (1989).
[12]K. Okuda, S. Kawamata, S. Noguchi, N. Itoh, and K. Kadowaki, J. Phys. Soc. Jpn. **60**, 3226 (1991).
[13]J. C. Martinez, S. H. Brongersma, A. E. Koshelev, B. Ivlev, P. H. Kes, R. P. Griessen, D. G. de Groot, Z. Tarnavski, and A. A. Menovsky, Phys. Rev. Lett. **69**, 2276 (1992).
[14]K. E. Gray, R. T. Kampwirth, and D. E. Farrell, Phys. Rev. B **41**, 819 (1990).
[15]L. N. Bulaevskii, Zh. Eksp. Teor. Fiz. **64**, 2241 (1973) [Sov. Phys. JETP **37**, 1143 (1973)].
[16]J. R. Clem, M. W. Coffey, and Zh. Hao, Phys. Rev. B **44**, 2732 (1991).
[17]M. Tinkham, *Introduction to Superconductivity* (McGraw-Hill, New York, 1975).
[18]C. R. Hu, Phys. Rev. B **6**, 1756 (1972).
[19]J. R. Clem, J. Low Temp. Phys. **18**, 427 (1975).